Strike-Slip Fault-Generated Paleotsunamis in Lake Iznik (NW Türkiye) : Numerical Modeling Corroborated by Coastal Deposits

Muhammad Naveed Zafar, Denys Dutykh, Raphaël Paris, Renaldo Gastineau, Julia de Sigoyer, Edward Duarte, Nur Deniz Ünsal, Nicolas Harrichhausen, Simon Flavard, Mustafa Şahin, et al.

Geophysical Research Letters

RESEARCH LETTER
10.1029/2025GL117422

Strike-Slip Fault-Generated Paleotsunamis in Lake Iznik (NW Türkiye): Numerical Modeling Corroborated by Coastal Deposits

Muhammad Naveed Zafar[1,2], Denys Dutykh[3], Raphaël Paris[4], Renaldo Gastineau[1], Julia De Sigoyer[5], Edward Duarte[1], Nur Deniz Ünsal[6], Nicolas Harrichhausen[5,7], Simon Flavard[4], Mustafa Şahin[6], and Pierre Sabatier[1]

[1]EDYTEM, Université Savoie Mont-Blanc, CNRS, Le Bourget-du-Lac, France, [2]LAMA, University Grenoble Alpes, University Savoie Mont Blanc, CNRS, Chambéry, France, [3]Mathematics Department, Khalifa University of Science and Technology, Abu Dhabi, United Arab Emirates, [4]Laboratoire Magmas et Volcans, Université Clermont Auvergne, CNRS, IRD, OPGC, Clermont-Ferrand, France, [5]University Grenoble Alpes, University Savoie Mont Blanc, CNRS, IRD, IFSTTAR, Grenoble, France, [6]Fen-Edebiyat Fakültesi, Arkeoloji Bölümü, Görükle, Bursa Uludağ Üniversitesi, Bursa, Türkiye, [7]Department of Geological Sciences, University of Alaska Anchorage, Anchorage, Alaska, USA

Abstract Strike-slip faults in lacustrine environments present overlooked tsunamigenic potential. For the first time, we have reconstructed paleotsunamis triggered by strike-slip faulting with a dip-slip component that ruptured the lake floor. This study focuses on Lake Iznik (Türkiye), located along the middle strand of the North Anatolian Fault (MNAF). We modeled tsunami generation, propagation, and inundation for the 121 CE (Mw ~7.3) and 1065 CE (Mw ~6.9) earthquakes using a coupled coseismic dislocation and hydrodynamic model. Simulated run-ups and inundation distances are validated against coastal tsunami deposits. Our results show maximum run-ups of ~3 m for the 121 CE event and ~1 m for the 1065 CE event, highlighting the tsunami hazard to the lakeshore. We also demonstrate that the tsunami generated during the 1065 CE event lacked sufficient wave height (<0.5 m) to damage the newly discovered submerged Byzantine basilica. These findings emphasize the need to integrate tsunami risk into seismic hazard assessments for lacustrine strike-slip fault zones.

Plain Language Summary This study investigates the often-overlooked tsunami hazard from underwater strike-slip fault earthquakes in lakes. We focus on Lake Iznik in Türkiye, which lies along the middle strand of the North Anatolian Fault. Using computer simulations, along with geological and historical records, we reconstructed tsunamis generated by the 121 CE (Mw 7.3) and 1065 CE (Mw 6.9) earthquakes, which ruptured the floor of Lake Iznik. The 121 CE event produced waves up to 3 m high, inundating areas over 500 m inland, while the 1065 CE tsunami carried lower energy. We also show that the 1065 CE event did not damage a recently discovered submerged Byzantine basilica, which potentially hosted the First Council of Nicaea in 325 CE, a foundational event in early Christianity. We validated our numerical results using sediment layers deposited by past tsunamis along the lakeshore, confirming their accuracy. Earthquakes in this region occur roughly every 1,000 years, and since the last one was in 1065 CE, there is growing concern about a future earthquake and its associated tsunami potential. Our findings show that strike-slip faults beneath lakes can generate damaging tsunamis, and that these hazards should be integrated into future seismic risk assessments for lakeside communities.

Key Points:

- First reconstruction of strike-slip fault-generated palaeotsunamis rupturing a lake floor, validated by coastal tsunami deposits
- The 121 CE tsunami in Lake Iznik produced up to ~3 m run-up and over 500 m inundation, posing serious hazards to lakeshore communities
- The 1065 CE tsunami lacked sufficient wave height to damage the submerged basilica, providing new constraints on its collapse

Supporting Information:

Supporting Information may be found in the online version of this article.

Correspondence to:

M. N. Zafar,
Muhammad-Naveed.Zafar@univ-smb.fr

Citation:

Zafar, M. N., Dutykh, D., Paris, R., Gastineau, R., De Sigoyer, J., Duarte, E., et al. (2025). Strike-slip fault-generated paleotsunamis in Lake Iznik (NW Türkiye): Numerical modeling corroborated by coastal deposits. *Geophysical Research Letters*, *52*, e2025GL117422. https://doi.org/10.1029/2025GL117422

Received 4 JUN 2025
Accepted 4 SEP 2025

Author Contributions:

Conceptualization: Muhammad Naveed Zafar, Denys Dutykh, Julia De Sigoyer, Pierre Sabatier
Formal analysis: Muhammad Naveed Zafar
Investigation: Muhammad Naveed Zafar, Denys Dutykh, Raphaël Paris, Simon Flavard, Pierre Sabatier
Methodology: Muhammad Naveed Zafar, Denys Dutykh, Raphaël Paris
Project administration: Denys Dutykh, Pierre Sabatier

1. Introduction

Earthquake-induced tsunamis are among the most destructive natural hazards, causing the loss of hundreds of thousands of lives and trillions of dollars in damage to infrastructure and the environment over the past century (Swiss Re, 2024; UNDRR, 2017). These tsunamis are generated by rapid deformation of the seafloor due to fault displacement (Dutykh et al., 2006; Synolakis et al., 1997) and are traditionally associated with large subduction-zone earthquakes (Dias et al., 2014; Rashidi et al., 2018; Stein & Okal, 2005). However, recent events have demonstrated that strike-slip faults also possess significant tsunamigenic potential. Notable examples include the 2018 CE Mw 7.5 Palu earthquake, which generated maximum tsunami run-up of ~6 m (Carvajal et al., 2019; Elbanna et al., 2021); the 1999 CE Mw 7.4 Kocaeli earthquake, which occurred along the North Anatolian fault and triggered the Izmit Bay tsunami with a run-up of 1–3 m (Altinok et al., 2001; Tinti et al., 2006); and the 1994

Resources: Renaldo Gastineau, Julia De Sigoyer, Edward Duarte, Nur Deniz Ünsal, Nicolas Harrichhausen, Mustafa Şahin, Pierre Sabatier
Software: Muhammad Naveed Zafar
Supervision: Denys Dutykh, Pierre Sabatier
Validation: Muhammad Naveed Zafar
Writing – original draft: Muhammad Naveed Zafar
Writing – review & editing: Muhammad Naveed Zafar, Denys Dutykh, Raphaël Paris, Renaldo Gastineau, Julia De Sigoyer, Edward Duarte, Nur Deniz Ünsal, Nicolas Harrichhausen, Simon Flavard, Mustafa Şahin, Pierre Sabatier

CE Mw 7.1 Mindoro tsunami, which was likely amplified by subsequent landslides (Ramirez et al., 2022) and produced a maximum run-up of ∼7 m (Imamura et al., 1995). These cases highlight the need to investigate tsunami hazards associated with strike-slip fault systems, particularly in enclosed or semi-enclosed basins, where even moderate vertical displacement or secondary effects, such as landslides, can amplify the tsunami impact.

However, assessing tsunami hazards in regions with long recurrence intervals presents an additional challenge. To accurately estimate future tsunami hazards, understanding past events is important. Sediments serve as continuous archives that preserve geological records of past events. They thus offer valuable information about high-impact, low-frequency events that are rarely observed in instrumental or historical records (Kremer et al., 2021; Sabatier et al., 2022). Integrating these archives with numerical modeling enables researchers to reconstruct and validate past tsunami events and gain information about their occurrence, dynamics, and impacts on coastal communities (Kremer et al., 2015; Zafar et al., 2024, 2025). However, lacustrine paleotsunami deposits have been extensively overlooked compared to their marine counterparts, even though numerous paleotsunami events have been documented in lacustrine settings based on their geological signatures (Bozzano et al., 2009; Dirksen et al., 2011; Freundt et al., 2006; Kremer et al., 2012; Moore et al., 2014; Nigg et al., 2021; Schnellmann et al., 2002). Although the tsunamigenic potential of strike-slip earthquakes has been explored in recent studies (e.g., (Elbanna et al., 2021; Estrada et al., 2021), reconstructions of paleotsunamis associated with strike-slip faults in lake settings are still lacking, leaving a significant gap in hazard assessment and risk mitigation efforts.

To address these challenges, this study focuses on the middle strand of the North Anatolian Fault (MNAF), part of one of Earth's most seismically active strike-slip fault systems (NAF) (Şengör et al., 2005). Some segments of the western part of the MNAF, such as the Iznik fault, have remained seismically quiet since the 1065 CE earthquake, raising concerns about an impending rupture (Benjelloun et al., 2021; Gastineau et al., 2021). Large earthquakes (Mw > 7) along the Iznik fault have a recurrence interval of 970 ± 235 years (Duarte et al., 2023), suggesting that the region may soon experience another significant seismic event associated with potential tsunami hazards. The Iznik fault crosses the floor of Lake Iznik (Gastineau et al., 2021), where the historically important city of Nicaea (now Iznik) is located on its eastern shore, making it a crucial site for investigating paleotsunamis for future hazard assessment. Here, we present the first paleotsunami investigation at Lake Iznik, which integrates numerical modeling with stratigraphic, paleoseismological, and historical records. The numerical simulations are validated against tsunami deposits, identified in coastal lake sediment cores. This research provides new insights into tsunami hazards linked to the strike-slip fault at Lake Iznik and establishes a framework applicable to similar lacustrine environments worldwide.

2. Geological Settings and Previous Studies on the MNAF

The North Anatolian Fault Zone (NAFZ) is a ∼1,200 km-long, right-lateral strike-slip fault system accommodating the relative motion between the Eurasian and Anatolian plates (Şengör et al., 2005). The fault has a geodetic slip rate of approximately 24.5–26.5 mm/yr (e.g., Meade et al., 2002; Reilinger et al., 2006). It is relatively narrow in the east (Barka, 1996) but becomes more complex to the west as it enters the Marmara Sea. In the Marmara region, northwest Anatolia, the NAFZ diverges into three strands, each separated by ∼50 km (Şengör et al., 2005). The northern strand (NNAF), which extends beneath the Marmara Sea, accommodates the highest slip rate of ∼20–25 mm/yr (Okur et al., 2024). The middle (MNAF) and southern (SNAF) strands, running mostly inland and bounding several Quaternary basins, account for the remaining ∼20%–25% of the total slip (Okur et al., 2024). Among these, the MNAF is particularly debated because of its seismic quiescence in the instrumental period (Benjelloun et al., 2021; Gastineau et al., 2021). Additionally, it runs through the Lake Iznik, one of the largest freshwater lakes in Turkey, raising concerns about increased tsunami hazards in the region.

Lake Iznik lies in the southeastern part of the Marmara Sea. It has a maximum depth of ∼70 m and dimensions of approximately 12 km north–south and 32 km east–west. The lake is fed primarily by five rivers and drains via a single outlet, Gölyatağı Dere. Numerous paleoseismological studies have been conducted on the MNAF (Figure 1c). These studies revealed that the MNAF is partitioned in the Lake Iznik area into two main segments (Figure 1): one is the Gürle Fault (GF), which borders the southern bank of the lake and mostly affects the bedrock; the other is the Iznik Fault (IF), which has a rectilinear shape, runs into Lake Iznik, and affects the sedimentary layers of the lake. The IF primarily shows horizontal dextral slip with a minor normal component dipping southward (Gastineau et al., 2021). In contrast, the GF mainly has a normal component dipping northward

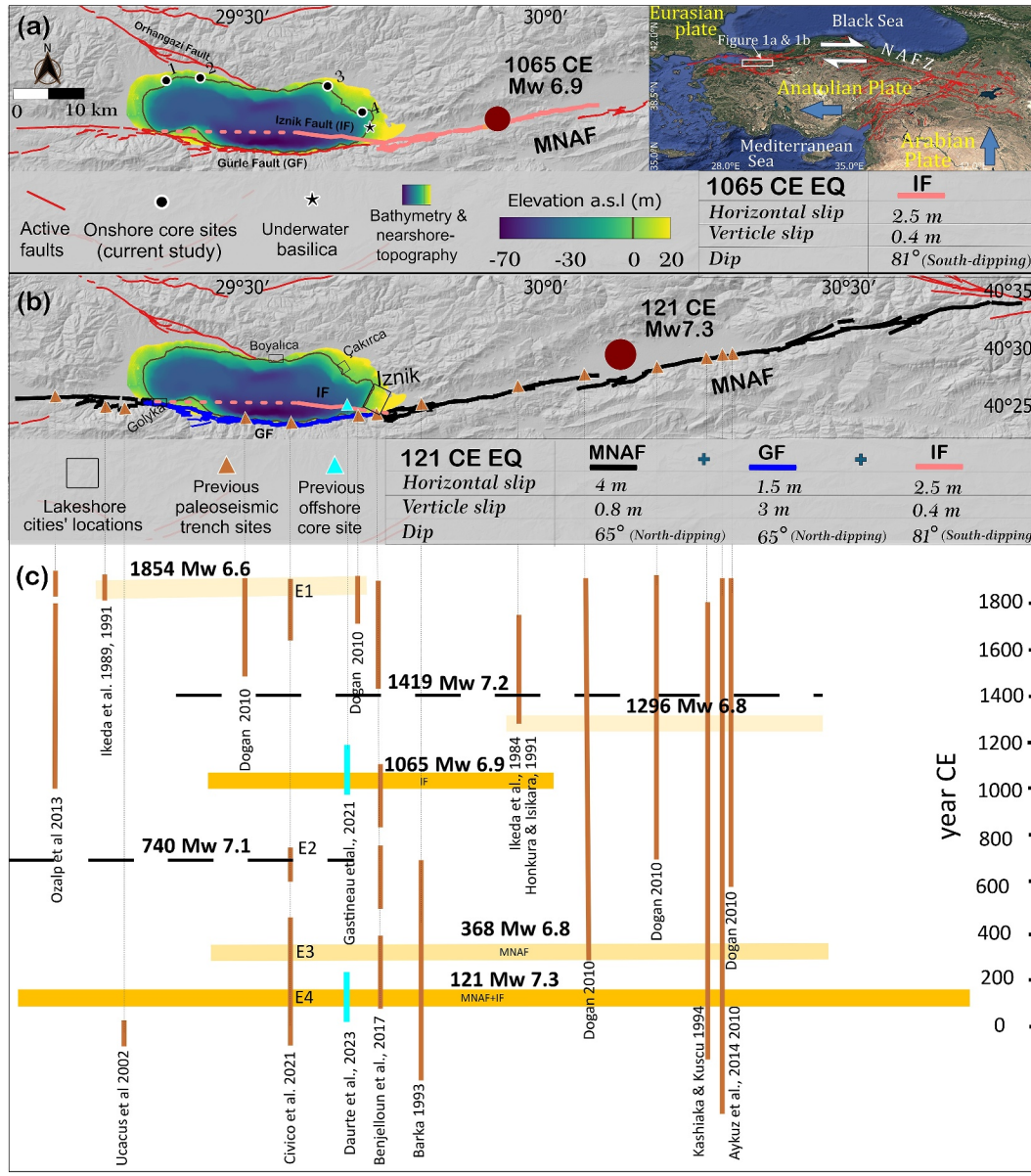

Figure 1. (a) Bathymetry and nearshore topography of Lake Iznik, illustrating the IF (pink), which ruptured during the 1065 CE earthquake. Black circles (1–4) indicate the onshore core sites analyzed in this study. (b) MNAF (black), including its GF segment (blue) and the IF segment (pink), which ruptured during the 121 CE earthquake. (c) Earthquakes scenario modified from Benjelloun et al. (2021) and Civico et al. (2021); vertical bars indicate the age ranges of paleoearthquake occurrences identified from previous trenches and core studies (corresponding to the triangles in panel b), whereas horizontal bars represent historical seismic events. The length of the horizontal bars represents the estimated rupture extent based on Wells and Coppersmith (1994). The fault parameters for both events are provided in their respective legends.

(Civico et al., 2021; Doğan et al., 2015). Together, these faults form a negative flower structure, which is responsible for the deepest basin in Lake Iznik (Benjelloun et al., 2021; Civico et al., 2021; Gastineau et al., 2021).

Over the past two millennia, the MNAF has generated at least six major earthquakes that caused significant damage to the city of Iznik, including the 29–32 CE (Mw 7), 121 CE (Mw 7.3), 368 CE (Mw 6.9), 740 CE (Mw 7.1), 1065 CE (Mw 6.9), and 1,296 (Mw 6.9) events (Ambraseys & Finkel, 1991; Benjelloun et al., 2021; Civico et al., 2021; Gastineau et al., 2021; Guidoboni et al., 1994). These earthquakes have ruptured several segments of the MNAF (Figure 1b). This study focuses on two key events that ruptured the floor of Lake Iznik: the most recent 1065 CE event and the largest historically documented 121 CE event, to assess their potential for tsunami

generation. The 1065 event ruptured the IF resulting in ∼2.5 m horizontal and ∼0.4 m vertical offsets of lacustrine sediments that were identified using seismic reflection data and sediment cores (Duarte et al., 2023; Gastineau et al., 2021). However, according to Civico et al. (2021), the onshore trench studies along the GF did not show evidence of this rupture, suggesting that the 1065 event may have been confined to the IF, and its eastern prolongation along the MNAF (Figure 1a). In contrast, the 121 CE earthquake shows clear evidence for rupturing both the IF and GF segments. The total horizontal slip along the MNAF is estimated at 4 m during the 121 CE event, which is divided between the GF and the IF as the fault approaches Lake Iznik (Civico et al., 2021; Duarte et al., 2023). The vertical offset is higher about 1–2 m (Civico et al., 2021) along the north-dipping GF, and the horizontal offset along GF is in the range of 3.2–4.7 mm/yr (Benjelloun et al., 2021). The slip parameters for both earthquakes are summarized in the legends of Figures 1a and 1b. The strike angles of all segments along the MNAF fault and its total length of 148 km were determined based on high-resolution satellite imagery (Benjelloun et al., 2021). This region is considered seismically shallow, with a locking depth of ∼4.2 ± 1.03 km for the middle strand near Lake Iznik, based on GPS geodetic modeling (Okur et al., 2024).

3. Methods

3.1. Coseismic Dislocation Model

The first step in modeling an earthquake-induced tsunami is the translation of coseismic slip into surface displacements. These displacements are then incorporated into the tsunami propagation model, where they serve as bathymetric changes during the simulation (Dutykh & Dias, 2009a; Zafar et al., 2025). To calculate the 3D displacement of the Earth's surface, we use the well-known Okada model (Okada, 1985). This model assumes that the Earth behaves as a perfectly elastic half-space and takes uniform slip on rectangular fault patches as input. The model determines surface displacements by solving the half-space problem via Green's functions. For complex fault geometries, the fault plane can be divided into multiple rectangular subfaults in the model; each could have different orientations and slip characteristics. The Okada model is applied to each subfault, and the resulting surface deformations are summed to obtain the final displacement field.

3.2. Tsunami Propagation and Inundation Model

We used a two-dimensional (2D) depth-averaged nonlinear shallow water equation (NSWE) model GeoClaw (Clawpack Development Team, 2020) to simulate tsunami wave propagation and inundation. GeoClaw is an open-source, widely recognized tsunami model that has been validated against the National Tsunami Hazard Mitigation Program (NTHMP) benchmark problems (González et al., 2011) and applied to numerous tsunami events with their comparisons to tide gauge (Adams & LeVeque, 2018) or geological data, including in alpine lakes (Zafar et al., 2024, 2025). GeoClaw employs a shock-capturing Godunov-type finite volume scheme (Dutykh et al., 2011; LeVeque, 2002) on rectangular grids with adaptive mesh refinement. It automatically handles dry states effectively during inundation. For a detailed description of GeoClaw, see LeVeque et al. (2011).

Although the Geoclaw model is primarily designed to account for vertical seafloor displacement above the fault line, we also include horizontal displacement by applying the Tanioka filter (Tanioka & Satake, 1996). This approach is based on the principle that horizontal displacement on a sloping bottom causes vertical motion proportional to the slope's magnitude. If the slope is small, this effect can be approximated mathematically using a first-order Taylor expansion:

$$u_h = u_1 h_x + u_2 h_y$$

where u_1 and u_2 are the horizontal displacement components, and where $h(x, y)$ represents the bathymetry function. The indices x and y denote spatial partial derivatives. The term u_h represents the vertical displacement induced by the horizontal movement of the slope, which we incorporated as a correction to the vertical displacement component in our model.

Additionally, the details of the instantaneous excitation and shallow water assumptions used in our tsunami model are discussed within the framework proposed by Abrahams et al. (2023) (Text S1 in Supporting Information S1).

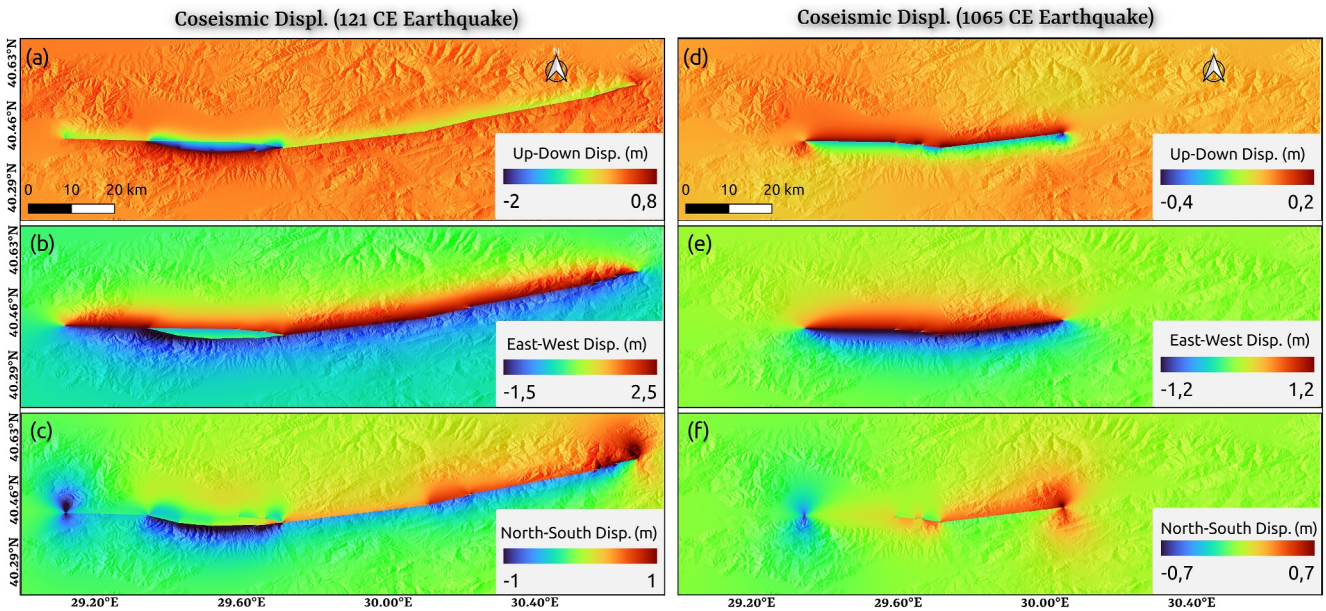

Figure 2. Vertical (up–down) and horizontal (east–west and north–south) components of surface displacement resulting from fault movement during the 121 CE earthquake (a–c) and the 1065 CE earthquake (d–f).

3.3. Tsunami Deposit Analysis

We surveyed 4 different sites around the shores of Iznik Lake to find traces of past tsunamis preserved in the sediments (Figure 1a). Thirteen stratigraphic logs were obtained by hand-held coring using an Edelman auger and a gouge auger at depths up to 3.3 m below the ground surface. The most convincing field evidence of tsunami deposits was found at the coring site 3 (north of Çakirca) on the northeastern shore of the lake. Laboratory analyses presented here are therefore focused on this site. Grain size analysis was performed on bulk sediment samples via a Beckman Coulter LS13230XR laser particle size analyzer at EDYTEM, with ultrasound during analysis.

The loss-on-ignition (LOI) was measured using the protocol of Heiri et al., 2001, with LOI550 and LOI950 used respectively as a proxy of organic matter (OM) and carbonate contents in the sediment. X-ray tomography was performed on specific sedimentary layers to characterize their structure in 3D. The samples were scanned at a tube voltage of 90 kV and a current of 62 µA using an EasyTom RX-Solutions CT-scan device at LMV. The 1,120 tomographic projections were reconstructed with a filtered back-projection algorithm, resulting in tomograms with a pixel resolution of 6.5 µm. A total of 3 samples of plant and organic remains were ^{14}C dated at LMC14 using accelerator mass spectrometry (Dumoulin et al., 2017). Calibration at 2σ was performed using the IntCal2020 calibration curve (Reimer et al., 2020).

4. Results

4.1. Earthquake-Induced Tsunami Simulations

4.1.1. Coseismic Displacement

We applied the Okada model to compute the three-dimensional coseismic displacements for the 121 CE and 1065 CE earthquakes, using the fault geometries and slip distributions as described in Section 2. In the 121 CE scenario, which involves rupture along both the IF and GF segments, the simulated vertical displacements ranged from −2.0 to 0.8 m (Figure 2a). The deepest basin of Lake Iznik experienced maximum subsidence, which aligned well with the present-day bathymetric profile. The 1065 CE earthquake, limited to the IF segment and its eastern prolongation along the MNAF, produced vertical displacements ranging from −0.4 to 0.2 m (Figure 2d). The horizontal displacement components corresponding to the 121 CE and 1065 CE events are presented in Figures 2b–2c and 2e–2f, respectively.

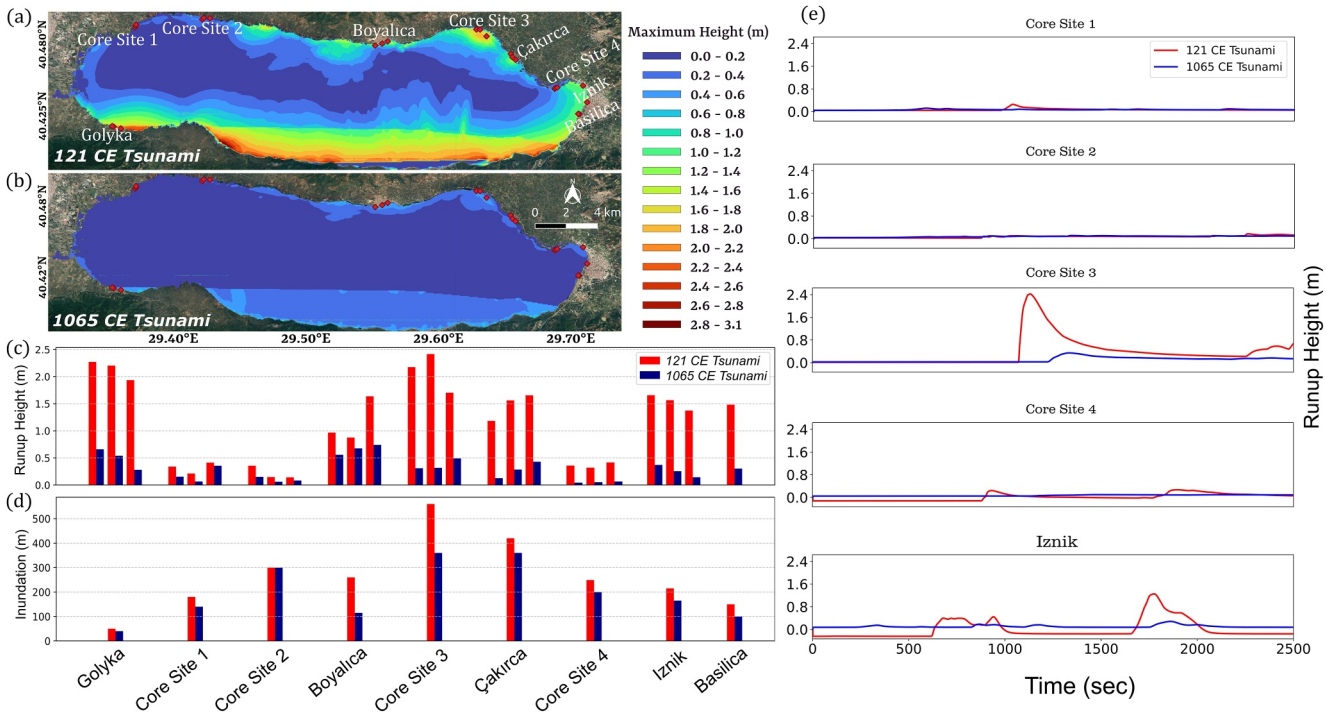

Figure 3. Maximum tsunami wave heights generated by the 121 CE (a) and 1065 CE (b) earthquakes over time. Run-up heights (c) and inundation distances (d) at locations marked by red diamonds in (a, b). Points are selected clockwise from Gölkaya to the Basilica. (e) Run-up time series at all core sites and at Iznik City.

4.1.2. Tsunami Wave Propagation and Inundation

The static coseismic displacements were incorporated into the tsunami model as instantaneous changes to the lake floor, which transform into the overlying water column and lead to the generation of tsunami waves. Tsunami propagation and inundation modeling was performed on a uniform rectangular grid with 10 m resolution, using high-resolution topographic and bathymetric data. To evaluate the influence of horizontal displacement, we ran simulations using (a) only the vertical displacement and (b) both the vertical and horizontal components (Figure S1 in Supporting Information S1). Due to the gentle slope of Lake Iznik's basin, with a maximum gradient of 7.5° (Figure S2 in Supporting Information S1), differences in wave height were negligible. Therefore, only the vertical displacement component was considered in the run-up analysis. We also tested downdip fault widths ranging from 5 to 12 km. The results revealed minimal variations in wave height and spatial distribution (Figure S3 in Supporting Information S1), and a 5 km width was selected for subsequent run-up simulations, which is consistent with the ∼4.2 ± 1.03 km locking-depth estimates from regional geodetic studies (Okur et al., 2024).

The spatial distributions of maximum tsunami wave heights for the 121 CE and 1065 CE events with modeled run-up heights and inundation distances at selected shoreline location are shown in Figures 3a–3d. Tsunami run-up time series for both events at the core sites and at Iznik city are shown in Figure 3e.

For the 121 CE simulation, tsunami wave propagation snapshots (Video S1) and time series (Figure 3e) show that the leading wave reached Iznik city within 10 min after the earthquake. The town was notably affected, with a modeled run-up height of up to ∼1.5 m (Figure 3c) and inundation reaching ∼200 m on land (Figure 3d). Moreover, the peak of the leading wave propagated toward the northeastern shore of the lake (location of core site 3), arriving within 18 min (Figure 3e; Video S1). At this site, the maximum run-up reached ∼2.5 m, with inundation extending beyond 500 m inland (Figures 3c and 3d). Other shoreline areas near core sites 1, 2, and 4 experienced lower tsunami height (Figures 3c and 3d). Among the populated sites, Gölyaka experienced the highest wave height (>2 m) but limited inundation, whereas Çakırca experienced the greatest inundation (>400 m), with run-up exceeding 1.5 m. Overall, the highest modeled tsunami height (∼3 m) was observed along the southern shore of the lake.

10.1029/2025GL117422

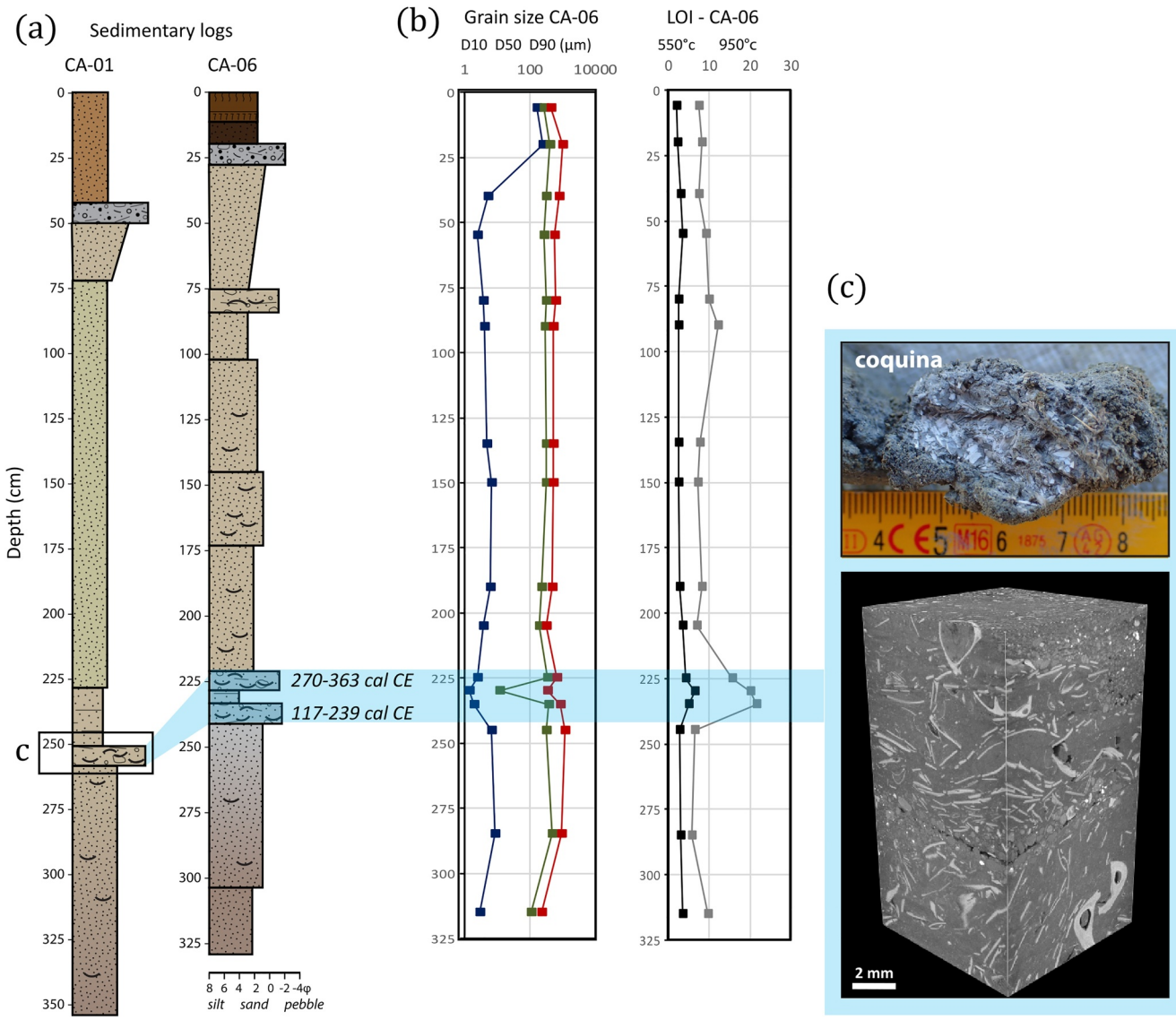

Figure 4. (a) Sedimentary sequences showing evidence of tsunami deposits in Lake Iznik shore sediments (site Çakirca, core site 3). Deposits interpreted as formed by tsunamis take the form of detrital shell-rich layers (e.g., at 75–80 cm and 225–230 cm depth on core CA-06, and at 260 cm depth on core CA-01); (b) Grain size and loss-on-ignition (LOI) downcore profiles of core CA-06; (c) Close-up and CT-scan views of a detrital shell-rich tsunami layer found at a depth of 260 cm on core CA-01.

For the 1065 CE tsunami simulation, Iznik city was affected by a relatively small wave, with a maximum run-up of ∼0.5 m and inundation reaching ∼150 m. At Çakırca and core site 3, inundation extended up to 350 m, with similar run-up heights of ∼0.5 m. The highest modeled wave height during this event (∼1 m) occurred along the southern shore of the lake.

4.2. Tsunami Deposits

Among the various onshore sedimentary sequences studied, only those from core site 3, located north of Çakirca, provided convincing evidence of tsunamis. The sequences are mainly composed of lacustrine clayey-silt to fine sand sediment, with variations in grain size and color reflecting variations of the lake level. Two types of coarser-grained layers are identified: (a) coarse sand layers with pebbles, corresponding to deposits of delta fans (usually in the upper part of the sequences), and (b) detrital shell-rich layers, typically 5–15 cm thick, including fine pebbles, charcoals, and bones. These shell-rich layers are intercalated in the carbonated silty sediments with relatively higher OM content typical of lacustrine deposit without any gradational transition (Figures 4a and 4b).

The abundance of shells is correlated with increased LOI950 and relatively coarse sediment (Figure 4b). These shell-rich deposits are usually found in high-energy coastal environments, but here they are found in shallow-water lake sediments deposited in a low-energy environment. Shells are also not found in a live position, they were transported and fragmented into small clasts a few mm in size. X-ray tomography (CT-scan) shows different types of bioclasts (bivalve shells mostly of the Dreissenidae family, gastropods, fish bones, etc.) densely packed in sand-to-silt sediment (Figure 4c). All these observations lead us to conclude that the shell-rich layers correspond to high-energy events capable of transporting and redepositing shells and sand a few meters deep in the lake. The shell-rich layers found at 225–230 cm depth and 75–80 cm depth in core CA-06, and at 260 cm depth in core CA-01 are thus interpreted as tsunami deposits. The age of the lower shell-rich layer on core CA-06 (225–230 cm depth) is bracketed by a ^{14}C age of 117–239 cal CE obtained on a plant fragment at 235 cm depth, and an age of 270–363 cal CE on another plant fragment at 225 cm depth. These ages are concordant with the 121 CE earthquake, within the uncertainties of the ^{14}C ages. We could not find any material suitable for dating at depths close to the upper shell-rich layer (75–80 cm depth), but it is younger.

5. Discussion and Conclusions

5.1. Validation With Tsunami Deposits

The validation of numerical simulations with field observations is essential because of the inherent uncertainties associated with paleotsunami studies (Kremer et al., 2021; Zafar et al., 2025). For the 121 CE event, the model results indicate that the peak of the leading tsunami wave was directed toward the northeastern shore of Lake Iznik (Figure 3e; Video S1). At this location (core site 3), we identified onshore tsunami deposits, characterized by sharp deposition of detrital shell-rich sedimentary layers intercalated in carbonated silty lake sediment (Figure 4), which is consistent with a high-energy event (Sabatier et al., 2022). According to ^{14}C ages, this deposit could correspond to the 121 CE event. In contrast, at other sites (core sites 1, 2, and 4), the modeled run-up heights remained below 0.5 m (Figure 3) with no evidence of shell-rich deposits. This evidence serves as strong validation of numerical modeling and the occurrence of a large tsunami in the northeastern part of the lake in 121 CE. This multidisciplinary approach, integrating numerical modeling with sedimentological validation, substantially advances the assessment of tsunami hazards in lacustrine environments, especially in regions affected by earthquakes with long recurrence intervals and lacking detailed historical records. These findings also highlight the importance of tsunami wave height and directivity in controlling the spatial distribution of tsunami deposits along lake shores, although other factors such as available sediment and accommodation space are also required to preserve tsunami deposits. Understanding these controls is essential, as such deposits serve as key indicators of both the occurrence and impacts of past tsunami events.

For the 1065 CE event, simulations indicate that the leading wave also propagated toward core site 3 (Figure 3; Video S2) but with considerably lower energy and a run-up wave height (∼0.5 m) compared to the 121 CE tsunami. In core CA-06, a minor carbonate peak with shell fragments was observed at 75–80 cm depth. Although no age control is available at this level, this thinner detrital shell-rich layer may represent a high-energy event similar to the 121 CE tsunami deposits but with a lower magnitude. We therefore suggest that the detrital layer at 75–80 cm depth could be related to the 1065 CE event.

5.2. Tsunamigenic Potential of Strike-Slip Faulting and Hazards

Our simulations indicate that the 121 CE earthquake generated tsunami waves with maximum run-up heights reaching ∼3 m and inundation extending over 500 m inland, posing a significant hazard to Lake Iznik's shoreline communities (Figure 3). Notably, the historical city of Iznik on the eastern shore experienced modeled run-up heights up to ∼1.5 m and inundation of ∼200 m (Figure 3).

Given that the 1065 CE and 121 CE earthquakes are historical events, their rupture propagation characteristics are poorly constrained, which challenges dynamic modeling. Our results, based on instantaneous excitation, indicate that horizontal slip contributed little; instead, most tsunamigenic potential in Lake Iznik arises from the vertical slip component (Figures S4 and S5 in Supporting Information S1). To quantify this, we performed tsunami energy calculations following Dutykh and Dias (2009b) (Figure S6 in Supporting Information S1). The peak tsunami wave energy for the scenario including vertical slip is 7.39×10^{11} J, nearly 90 times greater than the pure strike-slip case (8.13×10^{9} J).

However, strike-slip ruptures propagating through sedimentary layers, such as the 1065 CE and 121 CE events, may significantly enhance the fault vertical component of ground velocity, thereby increasing tsunamigenic potential (Abdelmeguid et al., 2025). Furthermore, seismic shaking from strike-slip ruptures can generate standing waves in lakes lasting several days, even without accounting for sediment amplification (Zafar et al., 2025), underscoring the high sensitivity of lacustrine basins to strong ground motion. Moreover, strike-slip ruptures in sedimentary basins may undergo localized supershear (Abdelmeguid et al., 2025), which under certain conditions can further increase the tsunami potential (Elbanna et al., 2021). This mechanism is particularly relevant to the 1065 CE rupture on the Iznik Fault, a rectilinear, predominantly strike-slip fault traversing the Lake Iznik sedimentary basin.

Thus, these studies suggest that tsunami generation could have been even more devastating beyond our estimates based on instantaneous excitation at Lake Iznik. Given the recurrence interval of 970 ± 235 years of large earthquakes in Lake Iznik along the MNAF (Duarte et al., 2023) and its seismic quiescence since 1065 CE (Gastineau et al., 2021), the likelihood of a future large earthquake and associated potential tsunami hazard may have increased. These results highlight the urgent need to incorporate inland tsunami scenarios into regional seismic hazard assessments and urban planning, particularly to protect densely populated lakeshore areas.

5.3. Submerged Basilica

Among the most important cultural landmarks is the submerged Basilica of Saint Neophytos, which was discovered in 2014 along the eastern shore of Lake Iznik (Şahin & Fairchild, 2018). This basilica potentially hosted the First Council of Nicaea in 325 CE, a foundational event in early Christianity (Şahin & Fairchild, 2018). Previous studies have proposed that the collapse of the basilica may have been caused by the 1065 CE earthquake or an associated tsunami (Gastineau et al., 2021). However, our tsunami simulations based on instantaneous excitation indicate that wave heights at the basilica site related to the 1065 CE earthquake were insufficient (<0.5 m) to cause structural damage.

Conflict of Interest

The authors declare no conflicts of interest relevant to this study.

Data Availability Statement

In our study, simulations were conducted using the hydrodynamic model GeoClaw, which is available on the Clawpack website (Clawpack Development Team, 2020). The simulation data are available under the Creative Commons Attribution-ShareAlike 4.0 International license in Zafar (2025). This repository includes all necessary output files and scripts to run and reproduce our simulation results.

Acknowledgments
This study was carried out as part of the "BASILIZNIK-SECRETS" project funded by the French ANR CE03-2019 BASILIZNIK-SECRETS, project. The authors would like to thank the Turkish Ministry of Culture and Tourism for permitting core sampling around Lake Iznik. MNZ gratefully acknowledges the financial support received from the MESRI and ED MSTII in the form of a PhD scholarship to conduct research for his doctoral thesis. We thank Farhan Javed for his help with the reconstruction of the fault geometry.

References

Abdelmeguid, M., Elbanna, A., & Rosakis, A. (2025). Ground motion characteristics of subshear and supershear ruptures in the presence of sediment layers. *Geophysical Journal International*, *240*(2), 967–987. https://doi.org/10.1093/gji/ggae422

Abrahams, L. S., Krenz, L., Dunham, E. M., Gabriel, A.-A., & Saito, T. (2023). Comparison of methods for coupled earthquake and tsunami modelling. *Geophysical Journal International*, *234*(1), 404–426. https://doi.org/10.1093/gji/ggad053

Adams, L. M., & LeVeque, R. J. (2018). Geoclaw model tsunamis compared to tide gauge results final report.

Altinok, Y., Tinti, S., Alpar, B., Yalçiner, A. C., Ersoy, Ş., Bortolucci, E., & Armigliato, A. (2001). The Tsunami of August 17, 1999 in Izmit Bay, Türkiye. *Natural Hazards*, *24*(2), 133–146. https://doi.org/10.1023/A:1011863610289

Ambraseys, N. n., & Finkel, C. f. (1991). Long-term seismicity of Istanbul and of the Marmara Sea region. *Terra Nova*, *3*(5), 527–539. https://doi.org/10.1111/j.1365-3121.1991.tb00188.x

Barka, A. (1996). Slip distribution along the North Anatolian fault associated with the large earthquakes of the period 1939 to 1967. *Bulletin of the Seismological Society of America*, *86*(5), 1238–1254. https://doi.org/10.1785/BSSA0860051238

Benjelloun, Y., Julia, D. S., Garambois, S., Carcaillet, J., & Klinger, Y. (2021). Segmentation and Holocene behavior of the middle strand of the North Anatolian fault (NW Türkiye). https://doi.org/10.1002/essoar.10506809.1

Bozzano, F., Mazzanti, P., Anzidei, M., Esposito, C., Floris, M., Fasani, G. B., & Esposito, A. (2009). Slope dynamics of Lake Albano (Rome, Italy): Insights from high resolution bathymetry. *Earth Surface Processes and Landforms*, *34*(11), 1469–1486. https://doi.org/10.1002/esp.1832

Carvajal, M., Araya-Cornejo, C., Sepúlveda, I., Melnick, D., & Haase, J. S. (2019). Nearly instantaneous Tsunamis following the Mw 7.5 2018 Palu earthquake. *Geophysical Research Letters*, *46*(10), 5117–5126. https://doi.org/10.1029/2019GL082578

Civico, R., Smedile, A., Pantosti, D., Cinti, F. R., De Martini, P. M., Pucci, S., et al. (2021). New trenching results along the İznik segment of the central strand of the North Anatolian fault (Türkiye): An integration with preexisting data. *Mediterranean Geoscience Reviews*, *3*(1), 115–128. https://doi.org/10.1007/s42990-021-00054-9

Clawpack Development Team. (2020). Tsunami numerical code GeoClaw [Software]. *Clawpack Development Team*. Retrieved from https://www.clawpack.org/geoclaw

Dias, F., Dutykh, D., O'Brien, L., Renzi, E., & Stefanakis, T. (2014). On the modelling of tsunami generation and tsunami inundation. *Procedia IUTAM*, *10*, 338–355. https://doi.org/10.1016/j.piutam.2014.01.029

Dirksen, O., van den Bogaard, C., Danhara, T., & Diekmann, B. (2011). Tephrochronological investigation at Dvuh-Yurtochnoe Lake area, Kamchatka: Numerous landslides and Lake tsunami, and their environmental impacts. *Quaternary International*, *246*(1), 298–311. https://doi.org/10.1016/j.quaint.2011.08.032

Doğan, B., Tüysüz, O., & Şanlı, F. B. (2015). Tectonostratigraphic evolution of the basins on the southern branch of the North Anatolian fault system in the SE Marmara region, Türkiye. *International Journal of Earth Sciences*, *104*(2), 389–418. https://doi.org/10.1007/s00531-014-1083-9

Duarte, E., Sabatier, P., De Sigoyer, J., Gastineau, R., Anselmetti, F., Rapuc, W., et al. (2023). Long-term lacustrine paleoseismicity along the Middle strand of the North Anatolian Fault (MNAF), NW Türkiye. *AGU Fall Meeting Abstracts, 2023*. NH22A-03 https://ui.adsabs.harvard.edu/abs/2023AGUFMNH22A..03D/abstract

Dumoulin, J.-P., Comby-Zerbino, C., Delqué-Količ, E., Moreau, C., Caffy, I., Hain, S., et al. (2017). Status report on sample preparation protocols developed at the LMC14 laboratory, saclay, France: From sample collection to 14C AMS measurement. *Radiocarbon*, *59*(3), 713–726. https://doi.org/10.1017/RDC.2016.116

Dutykh, D., & Dias, F. (2009a). Tsunami generation by dynamic displacement of sea bed due to dip-slip faulting. *Mathematics and Computers in Simulation*, *80*(4), 837–848. https://doi.org/10.1016/j.matcom.2009.08.036

Dutykh, D., & Dias, F. (2009b). Energy of tsunami waves generated by bottom motion. *Proceedings of the Royal Society A: Mathematical, Physical and Engineering Sciences*, *465*(2103), 725–744. https://doi.org/10.1098/rspa.2008.0332

Dutykh, D., Dias, F., & Kervella, Y. (2006). Linear theory of wave generation by a moving bottom. *Comptes Rendus Mathematique*, *343*(7), 499–504. https://doi.org/10.1016/j.crma.2006.09.016

Dutykh, D., Poncet, R., & Dias, F. (2011). The VOLNA code for the numerical modeling of tsunami waves: Generation, propagation and inundation. *European Journal of Mechanics—B: Fluids*, *30*(6), 598–615. https://doi.org/10.1016/j.euromechflu.2011.05.005

Elbanna, A., Abdelmeguid, M., Ma, X., Amlani, F., Bhat, H. S., Synolakis, C., & Rosakis, A. J. (2021). Anatomy of strike-slip fault tsunami genesis. *Proceedings of the National Academy of Sciences*, *118*(19), e2025632118. https://doi.org/10.1073/pnas.2025632118

Estrada, F., González-Vida, J. M., Peláez, J. A., Galindo-Zaldívar, J., Ortega, S., Macías, J., et al. (2021). Tsunami generation potential of a strike-slip fault tip in the westernmost Mediterranean. *Scientific Reports*, *11*(1), 16253. https://doi.org/10.1038/s41598-021-95729-6

Freundt, A., Kutterolf, S., Wehrmann, H., Schmincke, H.-U., & Strauch, W. (2006). Eruption of the dacite to andesite zoned Mateare Tephra, and associated tsunamis in Lake Managua, Nicaragua. *Journal of Volcanology and Geothermal Research*, *149*(1), 103–123. https://doi.org/10.1016/j.jvolgeores.2005.06.001

Gastineau, R., Julia, D. S., Sabatier, P., Fabbri, S., Anselmetti, F., Develle, A.-L., et al. (2021). Active subaquatic fault segments in Lake Iznik along the middle strand of the North Anatolian fault, NW Türkiye. *Tectonics*, *40*(1), e2020TC006404. https://doi.org/10.1029/2020TC006404

González, F., LeVeque, R. J., Varkovitzky, J., Chamberlain, P., Hirai, B., & George, D. L. (2011). *GeoClaw results for the NTHMP tsunami benchmark problems*. Results of the 2011 NTHMP Model Benchmarking Workshop.

Guidoboni, E., Traina, G., & Comastri, A. (1994). Catalogue of ancient earthquakes in the Mediterranean Sea up to the 10th century. *ITA*. https://iris.unisalento.it/handle/11587/112165

Heiri, O., Lotter, A. F., & Lemcke, G. (2001). Loss on ignition as a method for estimating organic and carbonate content in sediments: Reproducibility and comparability of results. *Journal of Paleolimnology*, *25*(1), 101–110. https://doi.org/10.1023/A:1008119611481

Imamura, F., Synolakis, C. E., Gica, E., Titov, V., Listanco, E., & Lee, H. J. (1995). Field survey of the 1994 Mindoro Island, Philippines tsunami. *Pure and Applied Geophysics*, *144*(3), 875–890. https://doi.org/10.1007/BF00874399

Kremer, K., Anselmetti, F. S., Evers, F. M., Goff, J., & Nigg, V. (2021). Freshwater (Paleo) tsunamis – A review. *Earth-Science Reviews*, *212*, 103447. https://doi.org/10.1016/j.earscirev.2020.103447

Kremer, K., Hilbe, M., Simpson, G., Decrouy, L., Wildi, W., & Girardclos, S. (2015). Reconstructing 4000 years of mass movement and tsunami history in a deep peri-Alpine Lake (Lake Geneva, France-Switzerland). *Sedimentology*, *62*(5), 1305–1327. https://doi.org/10.1111/sed.12190

Kremer, K., Simpson, G., & Girardclos, S. (2012). Giant Lake Geneva tsunami in AD 563. *Nature Geoscience*, *5*(11), 756–757. https://doi.org/10.1038/ngeo1618

LeVeque, R. J. (2002). *Finite volume methods for hyperbolic problems* (Vol. 31). Cambridge University Press. Retrieved from https://books.google.com/books?hl=en&lr=&id=QazcnD7GUoUC&oi=fnd&pg=PR17&dq=LeVeque,+2002&ots=W0ywwhVO-i&sig=kXgdNvnDIBQsPqYGc6Jh1csaQ88

LeVeque, R. J., George, D. L., & Berger, M. J. (2011). Tsunami modelling with adaptively refined finite volume methods. *Acta Numerica*, *20*, 211–289. https://doi.org/10.1017/S0962492911000043

Meade, B. J., Hager, B. H., McClusky, S. C., Reilinger, R. E., Ergintav, S., Lenk, O., et al. (2002). Estimates of seismic potential in the Marmara Sea region from block models of secular deformation constrained by global positioning system measurements. *Bulletin of the Seismological Society of America*, *92*(1), 208–215. https://doi.org/10.1785/0120000837

Moore, J. G., Schweickert, R. A., & Kitts, C. A. (2014). Tsunami-generated sediment wave channels at Lake Tahoe, California-Nevada, USA. *Geosphere*, *10*(4), 757–768. https://doi.org/10.1130/GES01025.1

Nigg, V., Wohlwend, S., Hilbe, M., Bellwald, B., Fabbri, S. C., de Souza, G. F., et al. (2021). A tsunamigenic Delta collapse and its associated tsunami deposits in and around Lake Sils, Switzerland. *Natural Hazards*, *107*(2), 1069–1103. https://doi.org/10.1007/s11069-021-04533-y

Okada, Y. (1985). Surface deformation due to shear and tensile faults in a half-space. *Bulletin of the Seismological Society of America*, *75*(4), 1135–1154. https://doi.org/10.1785/BSSA0750041135

Okur, Y., Bulut, F., & Garagon, A. (2024). Slip partitioning between subparallel strands of the North Anatolian fault in the Marmara region. *Geophysical Journal International*, *236*(1), 349–361. https://doi.org/10.1093/gji/ggad433

Ramirez, A. B. G., Ramos, N. T., Nawanao, L. P., Mangahas-Flores, R. Z., Narag, I. C., Baba, T., et al. (2022). An earthquake-triggered submarine mass failure mechanism for the 1994 Mindoro tsunami in the Philippines: Constraints from numerical modeling and submarine geomorphology. *Frontiers in Earth Science*, *10*, 1067002. https://doi.org/10.3389/feart.2022.1067002

Rashidi, A., Shomali, Z. H., Dutykh, D., & Keshavarz Faraj Khah, N. (2018). Evaluation of tsunami wave energy generated by earthquakes in the Makran subduction zone. *Ocean Engineering*, *165*, 131–139. https://doi.org/10.1016/j.oceaneng.2018.07.027

Reilinger, R., McClusky, S., Vernant, P., Lawrence, S., Ergintav, S., Cakmak, R., et al. (2006). GPS constraints on continental deformation in the Africa-Arabia-Eurasia continental collision zone and implications for the dynamics of plate interactions. *Journal of Geophysical Research*, *111*(B5). https://doi.org/10.1029/2005JB004051

Reimer, P. J., Austin, W. E. N., Bard, E., Bayliss, A., Blackwell, P. G., Ramsey, C. B., et al. (2020). The IntCal20 Northern hemisphere radiocarbon age calibration curve (0–55 cal kBP). *Radiocarbon*, *62*(4), 725–757. https://doi.org/10.1017/RDC.2020.41

Sabatier, P., Moernaut, J., Bertrand, S., Van Daele, M., Kremer, K., Chaumillon, E., & Arnaud, F. (2022). A review of event deposits in Lake sediments. *Quaternary*, *5*(3), 34. https://doi.org/10.3390/quat5030034

Šāhīn, M., & Fairchild, M. R. (2018). Nicea's underwater basilica. *Biblical Archaeology Review*, *44*(6). https://www.researchgate.net/publication/328466215_Nicea's_Underwater_Basilica

Schnellmann, M., Anselmetti, F. S., Giardini, D., McKenzie, J. A., & Ward, S. N. (2002). Prehistoric earthquake history revealed by lacustrine slump deposits. *Geology*, *30*(12), 1131–1134. https://doi.org/10.1130/0091-7613(2002)030<1131:PEHRBL>2.0.CO;2

Şengör, A. M. C., Tüysüz, O., İmren, C., Sakınç, M., Eyidoğan, H., Görür, N., et al. (2005). The North Anatolian fault: A new look. *Annual Review of Earth and Planetary Sciences*, *33*(33), 37–112. https://doi.org/10.1146/annurev.earth.32.101802.120415

Stein, S., & Okal, E. A. (2005). Speed and size of the Sumatra earthquake. *Nature*, *434*(7033), 581–582. https://doi.org/10.1038/434581a

Swiss Re Institute. (2024). The Indian Ocean tsunami: 20 years on, Swiss Re. Retrieved from https://www.swissre.com/institute/research/sigma-research/Economic-Insights/indian-ocean-tsunami-20-years-on.html

Synolakis, C., Liu, P., Philip, H. A., Carrier, G., & Yeh, H. (1997). Tsunamigenic sea-floor deformations. *Science*, *278*(5338), 598–600. https://doi.org/10.1126/science.278.5338.598

Tanioka, Y., & Satake, K. (1996). Tsunami generation by horizontal displacement of ocean bottom. *Geophysical Research Letters*, *23*(8), 861–864. https://doi.org/10.1029/96GL00736

Tinti, S., Armigliato, A., Manucci, A., Pagnoni, G., Zaniboni, F., Yalçiner, A. C., & Altinok, Y. (2006). The generating mechanisms of the August 17, 1999 İzmit Bay (Türkiye) tsunami: Regional (tectonic) and local (mass instabilities) causes. *Marine Geology*, *225*(1), 311–330. https://doi.org/10.1016/j.margeo.2005.09.010

United Nations Office for Disaster Risk Reduction (UNDRR). (2017). Tsunami hazard and risk assessment, UNDRR. Retrieved from https://www.undrr.org/publication/tsunami-hazard-and-risk-assessment

Wells, D. L., & Coppersmith, K. J. (1994). New empirical relationships among magnitude, rupture length, rupture width, rupture area, and surface displacement. *Bulletin of the Seismological Society of America*, *84*(4), 974–1002. https://doi.org/10.1785/BSSA0840040974

Zafar, M. N. (2025). Simulations data for strike-slip fault-generated Paleotsunamis in Lake Iznik (NW Türkiye): Numerical modeling corroborated by coastal deposits [Dataset]. *Zenodo*. https://doi.org/10.5281/zenodo.15583235

Zafar, M. N., Dutykh, D., Sabatier, P., Banjan, M., & Kim, J. (2024). Numerical reconstruction of landslide paleotsunami using geological records in alpine Lake aiguebelette. *Journal of Geophysical Research: Solid Earth*, *129*(5), e2023JB028629. https://doi.org/10.1029/2023JB028629

Zafar, M. N., Sabatier, P., Dutykh, D., Jomard, H., Rapuc, W., Lajeunesse, P., & Chapron, E. (2025). Modeling earthquake-induced seiche processes and subsequent homogenite deposition in lacustrine settings. *Earth and Planetary Science Letters*, *660*, 119348. https://doi.org/10.1016/j.epsl.2025.119348